The Dynamics of Interacting Elastic Filaments with Applications to Polymers and Biological Molecules

Aimee G. Bailey

Advisor: Adrian Sutton

Imperial College London

August 15, 2007

Abstract

The long-term goal of this research is to model the dynamics of many interacting, linear polymer chains in the bulk and at interfaces. The mechanical behavior is of primary interest, motivating a model that will permit access to system sizes greater than a few cubic nanometers and timescales on the order of milliseconds. Although molecular dynamics and Monte Carlo methods have been successfully employed to address many questions of polymer physics, the activation volumes for the molecular processes of interest far exceed approachable system sizes, given current computational technology. Continuum models have also been utilized; however, they fail to incorporate the molecular detail necessary to capture the physics behind phenomena resulting from long-chain molecular architecture, particularly at surfaces. One can hope to simulate the relevant mesoscopic and macroscopic processes by forgoing the inclusion of atomistic detail yet retaining tertiary structure of the molecules. A model is investigated here in which a polymer molecule is approximated as an elastic filament. The theoretical development of the resultant curve dynamics are described in detail.

Contents

1 Acknowledgements

Adrian Sutton, Advisor

Alvin Chua, PhD

The Thouron Award

National Science Foundation Graduate Research Fellowship Program (NSF GRFP)

2 Introduction

Pick any new piece of technology today and one can show how it almost invariably depends on polymers. Their development was largely driven by their desirable mechanical properties, namely synthetic rubbers for tires, but now the field has evolved to the point where they are serving nearly every material function. Organic semiconductors are replacing solid state materials to make organic light emitting diodes (OLEDs) [1, 2]. Short-chained polymers are being used for their birefringent optical properties for liquid crystal displays (LCDs) [3]. Adhesives are widely polymer based [4]. Their mechanical properties are more desirable than ever before. Combined with their light weight, plastics are an advantageous alternative to structural metals such as aluminum and steels for the aerospace industry [5, 6, 7, 8].

Plastics are indeed ubiquitous, but not necessarily in a bulk form. Any device which utilizes polymers will inevitably have multiple interfaces. Materials behave much differently when in a constrained situation such as near a surface, leading to distinct properties [9, 10, 11]. For instance, the useful mechanical attributes that are of interest to the aerospace industry are exhibited in nanocomposites, made by adding nanoparticles to a polymer matrix. When a high enough volume fraction of particles has been added, the majority of the matrix is in a constrained, non-bulk state. This coincides with when they exhibit an increased strength and toughness [12]. Very little is known about the interfacial processes responsible for this change of reaction, in part because the large systems are difficult to simulate with conventional methods.

We hope that research described herein will provide a means to narrow this gaping hole in current knowledge. We believe that we will be able to study the mechanical and interfacial

properties by simulating a coarse-grained model system. In doing so, we can hope that in the future stronger adhesives can be made, longer-lasting OLEDs and LCDs be built, and more environmentally-friendly structural materials may be designed for high performance applications.

3 Background

3.1 Brief introduction to polymer science

Polymers barely need an introduction. As we all know, their molecular structure is formed by repeating a monomer unit many times in succession, where each is attached to one another by strong covalent bonds. A polymer's identity and properties depend upon the chemistry of the repeat unit. Examples of natural polymers are rubbers, cellulose, DNA, and proteins. Synthetic polymers include commercial plastics such as nylon, kevlar, teflon, and the many derivatives of polyethylene.

Plastics are notorious for having both liquid-like and solid-like properties. At a high temperature, a plastic is in a viscoelastic melt, or rubbery state, with properties similar to that of silly putty — having mechanics which are highly strain-rate dependent with important relaxation times extending over very long time scales. As the temperature is lowered, the material experiences a second order phase transition referred to as the glass transition, occuring at a temperature (Tg), where the molecules lose mobility and become rigid, freezing the material in a particular configuration. Although we tend to think of plastics as amorphous, crystallization can actually take place in some systems before the Tg is reached. Upon cooling a partially-crystalline sample below the Tg, the material is then left frozen in a composite of crystallized regions in a matrix of glass. The Tg — and the Tm of crystals if they are present — is dependent upon the architecture, molecular weight, and chemical structure, in addition to the history of the sample [13, 14].

Molecular weight, or chain length, induces additional effects. At small molecular weights in a concentrated solution or a melt, individual chains predominantly stick to themselves. The resultant behavior is described by Rouse dynamics, where the molecules are short enough to be treated as an effective colloid undergoing Brownian motion. Above a critical molecular weight,

melts are pictorially described as a bowl of tangled spaghetti. The "tangles", an earmark of their unusual, elongated architecture, are important topological constraints referred to as entanglements. Current research supports the theories where entanglements are responsible for the viscoelastic properties of the melt state and the mechanical properties, such as crazing and strain hardening, of the glassy state [13, 14, 15, 16, 17, 18]. The most widely accepted theory describing the dynamics of polymers in an entangled melt state is the tube model, where the movement of polymer chains is restricted to a canal, an enclosure formed by the presence of other neighboring chains. The molecules resultantly move by a process called "reptation" through these arteries.

There are an infinite number of variations to the characteristic image of linear polyethylene that first comes to mind. One can add a cross-linking agent to create a network polymer referred to as a thermoset. Depending upon the type of synthesis, the chain architecture may already be branched, inhibiting any form of crystallization or order. The mechanical properties can be drastically changed by adding nanoparticles, to form a composite. The chemical identity of the repeat unit can be tuned for hydrophilicity, greater tensile strength, magnetic response, or better corrosion resistance, to name a few. Recently, a great deal of resources have been put toward research in the area of conducting and semi-conducting polymers. The potential is limitless.

One can say a great deal more about all of the branches and sub-branches of polymer science, but let us now restrict ourselves to the area of interest. Let us focus on the mechanical behavior of polymers of a linear architecture.

3.2 Simulations of polymers

Simulations have played an increasingly important role in the study of polymers. Permitted by the steadfast advancement in computer technology, computational modeling has established its place as a third branch of physics, alongside theoretical and experimental work. Simulations offer a new route towards understanding and predicting physical properties. Through modeling, we can now determine the intimate behavior of systems that are indistinguishable by the finest-tuned laboratory probe. Theories can now be tested and experiments interpreted in the virtual world.

Polymer science presents its own set of challenges to the field of computational physics. In particular, relevant processes take place over a large spectrum of size and length scales [15, 16, 17]. Relaxations times take place anywhere from 10^{-13} to 10^{-3} seconds, or days or weeks for a process such as creep. A ballpark number for an adequate system size needed to study a mechanical process can be determined by calculating the activation volume. For crystallographic, plastic events, that volume ranges from 3-7 nm^3 [19]. For a process in an amorphous, polymeric structure, one would expect this number to be larger since the concerted movement would have to extend over a larger amount of space.

Molecular dynamics (MD) has been used with great success. One of the first and most notable simulations was the observation of the transition from Rouse to reptation dynamics observed by Kremer, et. al., after 1500 hours of supercomputer time in 1988 [20]. Computers have come a long way since the late eighties, and other prominent research using MD has been put forward; however, it will be a long time yet before one can adequately model systems more than a few cubic nanometers in size for longer than microseconds, while retaining atomistic detail.

Coarse-grained models have also been proposed [24, 25, 26, 27, 28]. In some models, four to five molecular repeat units of a polymer have been treated as psuedo-particles and the dynamics of the system then investigated. The scaling behavior of these systems helps to render such approximations valid [18]. Further approximations have to be made in order to hope to explore problems happening in larger systems over longer time periods.

Monte Carlo (MC) has served as another powerful technique. New advanced algorithms have been conceived to treat dense systems with atomistic detail such as the concerted-rotation (ConRot), the configuration bias (CBMC), and the hybrid Monte Carlo (HMC) algorithms [21]. State of the art methods, however, do not yet approach polymers of realistic length, highlighting the difficulties of treating dense, constrained systems. Coarse-grained models treating molecules as a series of beads held together by springs in the spirit of Kremer and Grest [22] have also been investigated [23]; however, lattice models have to be used to make them computational feasible.

At the other end of the spectrum, some mechanical properties have been effectively studied using continuum mechanics [29]. Finite element method (FEM) in particular has been em-

ployed, where the plastic is treated as completely homogeneous, neglecting the chain nature of the material. Improvements in some models have been made such as accounting for anisotropy and structural rearrangements; chain texture can even be modeled throughout the course of a simulation [30, 31, 32]. However, FEM fails when one attempts to model an interface [33]. The molecules next to a surface undergo constrained rearrangements under stress, and the resultant mechanical properties differ greatly from those of the bulk. In some nanocomposites, where there is an extremely high surface to volume ratio, the organic matrix displays no "bulk" properties but is completely dominated by interfacial effects. FEM does not take this into account at present, but it is a technique which could be improved by incorporating results from microscopic mechanical experiments, such as the virtual ones proposed here.

In the hopes of creating a successful mesoscopic model to study the mechanical processes taking place in the regime between that now accessible by MD and continuum mechanics, it is evident that the tertiary structure of the molecule must be retained to capture the physics resulting from chain-like structure but gross approximations made to enhance computational viability.

3.3 Our approach

A technique used in biophysics to study bacterial cilia and stiff proteins is to approximate the object as a thin elastic filament and to model the dynamics due to elasticity, while including other forces that are of interest [34, 35, 36, 37]. This approximation is referred to as the Kratky-Porod wormlike chain model [38]. By treating molecules as continuous curves, atomistic detail is neglected but the long-chain nature of the material is preserved. For our case, the elastic filament is going to be assumed to have no cross-sectional area, reducing the problem to that of modeling space curve motion.

The ultimate goal of this research is to use this mesoscopic model to study size regimes, and their corresponding processes, between those accessible by finite element method and coarse-grained MD. Eventually, we hope to simulate a system of many molecules, although here we focus on the motion of one. In the remainder of this paper, I outline the theoretical developments of space curve dynamics to date. Some results are not applicable to our system of interest but could have significance in interfacial or biological systems. Theoretical results

are predominantly expressed for the 3D case but in parts are written out explicitly for 2D. Case studies are largely 2D for clarity.

4 Space curve Formalism and Geometrical Relations

Consider a finite, continuous space curve in R^3 parameterized by α, a general spatial coordinate, which spans the domain $[\alpha_{min}, \alpha_{max}]$. The coordinate α can be related to contour length by a metric, discussed below. Let us start with an arbitrary initial configuration. At time equals t_0, the position of the curve is given by $\mathbf{r}(\alpha, t_0)$, and the corresponding velocity is $\dot{\mathbf{r}}(\alpha, t_0)$. Within this paper, boldface type signifies a vector of the dimension of the space, and the $\{\dot{}\}$ denotes differentiation with respect to time.

At any coordinate value, α_0, one can define a local reference frame consisting of the orthonormal set of three vectors: the tangent, normal, and binormal. The tangent vector ($\hat{\mathbf{t}}$) points in a direction parallel to the curve; the normal vector ($\hat{\mathbf{n}}$) points in the direction of the second derivative; and the binormal vector ($\hat{\mathbf{b}}$) is calculated by taking the cross product of the tangent and normal.

4.1 Serret-Frenet relations

Given some initial configuration, the local reference frame, $\{\hat{\mathbf{t}},\hat{\mathbf{n}},\hat{\mathbf{b}}\}$, can be defined at any point along the space curve. If we find the local reference frame at n points equally spaced along the curve, the relationship between two neighboring reference frames, at α_i and α_{i+1} for instance, will depend on how much the underlying space curve is bending and spiraling.

There are two quantities which are used to characterize how the local reference frame rotates as one moves along the the space curve. The first, $\kappa(\alpha,\mathrm{t})$, represents the bend within the osculating plane, which is the plane formed by the tangent and normal vectors, $\left(\hat{\mathbf{t}} \times \hat{\mathbf{n}}\right)$. The second quantity, $\tau(\alpha,\mathrm{t})$, is the bend out of this plane. For example, a circle in 3D space has a constant κ as a function of α and a constant, zero-valued τ. A helix, on the other hand, has both constant and non-zero values of κ and τ.

The equations relating κ and τ and $\{\ \hat{\mathbf{t}}(\alpha,\mathrm{t}),\ \hat{\mathbf{n}}(\alpha,\mathrm{t}),\ \hat{\mathbf{b}}(\alpha,\mathrm{t})\}$ are the Serret-Frenet relations. Written in equation form, they are the following:

$$\frac{\partial \mathbf{r}}{\partial \alpha} = \hat{\mathbf{t}}, \quad \frac{\partial \hat{\mathbf{t}}}{\partial \alpha} = \kappa \hat{\mathbf{n}}, \quad \frac{\partial \hat{\mathbf{n}}}{\partial \alpha} = -\kappa \hat{\mathbf{t}} + \tau \hat{\mathbf{n}}, \quad \frac{\partial \hat{\mathbf{b}}}{\partial \alpha} = -\tau \hat{\mathbf{n}}. \tag{1}$$

Expressed in terms of a matrix, we have:

$$\frac{\partial}{\partial \alpha} \begin{pmatrix} \hat{t} \\ \hat{n} \\ \hat{b} \end{pmatrix} = \begin{pmatrix} 0 & \kappa & 0 \\ -\kappa & 0 & \tau \\ 0 & -\tau & 0 \end{pmatrix} \begin{pmatrix} \hat{t} \\ \hat{n} \\ \hat{b} \end{pmatrix}. \tag{2}$$

These equations hold at any α and at any instant t. In addition to being continuous, the space curve must also have continuous first and second derivatives, so that κ and τ are well-defined at every point.

4.2 Relation between α and contour length

It is important to note here what α, κ, and τ actually represent. As discussed above, equations written in terms of the general spatial coordinate, α, can be related to their corresponding form written in terms of contour length, s, by a metric. The metric is essentially a rule stick, telling the physical distance that is represented by a distance expressed in terms of α. Mathematically, it is determined by $g = (r_\alpha \cdot r_\alpha)$. Correspondingly, κ and τ in this report do not represent real curvature and torsion, but are related to these values, respectively, by $\tilde{\kappa} = \kappa g^{-\frac{1}{2}}$ and $\tilde{\tau} = \tau g^{-\frac{1}{2}}$, since $g^{-\frac{1}{2}} \frac{\partial}{\partial \alpha} = \frac{\partial}{\partial s}$. The Serret-Frenet relations are typically expressed in terms of $\tilde{\kappa}$, $\tilde{\tau}$, and derivatives with respect to contour length; however, they are just as true in the more general form written above. By treating the metric explicitly, we are preserving the opportunity to model extensibility and growth. We will return to the contour length representation in *Section 8.2*.

5 Dissipative Curve Dynamics

We would like to model an elastic filament in the low-Reynolds number regime, where dissipation dominates and inertial terms can be neglected [36]. The equation of motion for the underlying space curve can be derived by using the principle of least action [39]. One can do so in a dissipative framework by using a Raleigh dissipation function, R. Given R and some

Lagrangian, L, the equation of motion is,

$$\frac{d}{dt}\frac{\partial L}{\partial \dot{\mathbf{r}}} - \frac{\partial L}{\partial \mathbf{r}} = -\frac{\partial R}{\partial \dot{\mathbf{r}}}. \tag{3}$$

R is given by,

$$R = \frac{\zeta}{2}\int_{\alpha_{min}}^{\alpha_{max}} g^{\frac{1}{2}} \left|\dot{\mathbf{r}}\right|^2 d\alpha. \tag{4}$$

Using this form of R and neglecting inertial terms, *Equation 3* becomes,

$$-\frac{\partial L}{\partial \mathbf{r}} = \zeta g^{\frac{1}{2}}\ \dot{\mathbf{r}}. \tag{5}$$

Rewritten in terms of the force components resolved in the local Serret-Frenet Frame, {W,U,V},

$$\zeta\dot{\mathbf{r}} = -g^{-\frac{1}{2}}\ \frac{\delta E}{\delta r}\ = W\hat{t} + U\hat{n} + V\hat{b}, \tag{6}$$

where the Lagrangian reduces to -E, where E is the elastic bending energy.

6 Evolution of g, κ, τ, and the Serret-Frenet Frame

The evolution of g, κ, and τ can be determined in terms of {W,U,V}, the resolved force components. If one has g, κ, and τ, the curve can be completely reconstructed up to a translation and/or rotation. Therefore, by evolving these quantities, we will establish the evolution of the space curve.

6.1 Determination of $\dot{g}$ and $\dot{\hat{\mathbf{t}}}$

To get $\dot{g}$, differentiate the equation of motion, *Equation 6*, with respect to α and use the Serret-Frenet relations to get,

$$\zeta\frac{\partial\dot{\mathbf{r}}}{\partial\alpha}\ = (W_\alpha - \kappa U)\ \hat{\mathbf{t}} + (U_\alpha - \tau V + \kappa W)\ \hat{\mathbf{n}} + (V_\alpha + \tau U)\ \hat{\mathbf{b}}. \tag{7}$$

Using compatibility of temporal and spatial derivatives, *Equation 7* can be rewritten as,

$$\zeta\partial_t\left(g^{\frac{1}{2}}\,\hat{\mathbf{t}}\right) = (W_\alpha - \kappa U)\ \hat{\mathbf{t}} + (U_\alpha - \tau V + \kappa W)\ \hat{\mathbf{n}} + (V_\alpha + \tau U)\ \hat{\mathbf{b}}. \tag{8}$$

The evolution of the metric can be taken as the magnitude of the tangential component,

$$\zeta\dot{g} = 2g^{\frac{1}{2}}\ (W_\alpha - \kappa U)\,. \tag{9}$$

The remaining components - namely, the normal and binormal - define the evolution of the tangent vector.

$$\zeta\dot{\hat{\mathbf{t}}} = g^{-\frac{1}{2}}(U_\alpha - \tau V + \kappa W)\ \hat{\mathbf{n}} + g^{-\frac{1}{2}}(V_\alpha + \tau U)\ \hat{\mathbf{b}}. \tag{10}$$

6.2 Determination of $\dot{\kappa}$ and $\dot{\hat{\mathbf{n}}}$

To get $\dot{\kappa}$, first differentiate *Equation 10*, with respect to α and use the Serret-Frenet relations to get,

$$\begin{aligned}\zeta\partial_\alpha\dot{\hat{\mathbf{t}}} = -\frac{1}{2}\,g_\alpha g^{-\frac{3}{2}}\left[(U_\alpha + W\kappa - \tau V)\,\hat{\mathbf{n}} + (V_\alpha + \tau U)\,\hat{\mathbf{b}}\right] + g^{-\frac{1}{2}}\left[(U_{\alpha\alpha} + \kappa W_\alpha + \kappa_\alpha W - \tau V_\alpha - \tau_\alpha V)\,\hat{\mathbf{n}}\right.\\ \left. + (V_{\alpha\alpha} + \tau U_\alpha + \tau_\alpha U)\,\hat{\mathbf{b}} + (U_\alpha + \kappa W - \tau V)\left(-\kappa\hat{\mathbf{t}} + \tau\hat{\mathbf{b}}\right) - (V_\alpha + \tau U)\,(\tau\hat{\mathbf{n}})\right].\end{aligned} \tag{11}$$

It is also known that,

$$\zeta\partial_\alpha\dot{\hat{\mathbf{t}}} = \zeta\partial_t(\kappa\hat{\mathbf{n}}) = \zeta(\dot{\kappa}\hat{\mathbf{n}} + \kappa\dot{\hat{\mathbf{n}}}). \tag{12}$$

Equating the normal components will give us $\dot{\kappa}$.

$$\zeta\dot{\kappa} = -\frac{1}{2}\,g_\alpha g^{-\frac{3}{2}}\,(U_\alpha + W\kappa - \tau V) + g^{-\frac{1}{2}}\left(U_{\alpha\alpha} + \kappa W_\alpha + \kappa_\alpha W - 2\tau V_\alpha - \tau_\alpha V - \tau^2 U\right). \tag{13}$$

The remaining components constitute the evolution of the normal vector.

$$\zeta\dot{\hat{\mathbf{n}}} = \frac{1}{\kappa}\left[-\frac{1}{2}\,g_\alpha g^{-\frac{3}{2}}\,(V_\alpha + \tau U) + g^{-\frac{1}{2}}\left(V_{\alpha\alpha} + 2\tau U_\alpha + \tau_\alpha U + \tau\kappa W - \tau^2 V\right)\right]\hat{\mathbf{b}} - g^{-\frac{1}{2}}\,(U_\alpha + \kappa W - \tau V)\,\hat{\mathbf{t}}. \tag{14}$$

6.3 Determination of $\dot{\tau}$ and $\dot{\hat{\mathbf{b}}}$

To get an equation for $\dot{\tau}$, one can use a similar approach. Start with equation *Equation 14*:

$$\zeta\dot{\hat{\mathbf{n}}} = \frac{1}{\kappa}\left[-\frac{1}{2}\,g_\alpha g^{-\frac{3}{2}}\,(V_\alpha + \tau U) + g^{-\frac{1}{2}}\left(V_{\alpha\alpha} + 2\tau U_\alpha + \tau_\alpha U + \tau\kappa W - \tau^2 V\right)\right]\hat{\mathbf{b}} - g^{-\frac{1}{2}}\,(U_\alpha + \kappa W - \tau V)\,\hat{\mathbf{t}}. \tag{15}$$

Stepping back, we also have the following equation,

$$\zeta\left(\partial_\alpha\dot{\hat{\mathbf{n}}}\right) = \zeta\left(\partial_t(\hat{\mathbf{n}}_\alpha)\right) = \zeta\left(-\dot{\kappa}\hat{\mathbf{t}} - \kappa\dot{\hat{\mathbf{t}}} + \dot{\tau}\hat{\mathbf{b}} + \tau\dot{\hat{\mathbf{b}}}\right). \tag{16}$$

One can determine $\dot{\tau}$ by equating the binormal components of the right hand side of *Equation 16*, including the contribution from $\dot{\hat{\mathbf{t}}}$, and the derivative with respect to α of *Equation 15*. The

result is,

$$\zeta\dot{\tau} = \partial_\alpha \left[\frac{1}{\kappa}\left[-\frac{1}{2}\, g_\alpha g^{-\frac{3}{2}}\, (V_\alpha + \tau U) + g^{-\frac{1}{2}}\, \left(V_{\alpha\alpha} + 2\tau U_\alpha + \tau_\alpha U + \tau\kappa W - \tau^2 V\right)\right]\right] + g^{-\frac{1}{2}}\, (\kappa V_\alpha + \kappa\tau U)\,. \tag{17}$$

Following the same procedure, the evolution for $\dot{\hat{\mathbf{b}}}$ is,

$$\zeta\dot{\hat{\mathbf{b}}} = -g^{-\frac{1}{2}}\, (\tau U + V_\alpha)\, \hat{\mathbf{t}} + \frac{1}{\kappa}\left[\frac{1}{2} g_\alpha g^{-\frac{3}{2}}\, (V_\alpha + \tau U) - g^{-\frac{1}{2}}\, \left(V_{\alpha\alpha} + 2\tau U_\alpha + \tau_\alpha U + \tau\kappa W - \tau^2 V\right)\right] \hat{\mathbf{n}}. \tag{18}$$

The above evolution equations were determined using only Serret-Frenet behavior and are otherwise completely general. One simply needs to determine the forces on the curve, {W,U,V}, in order to determine the evolution of the metric, curvature, and torsion, and the Serret-Frenet frame, if it is desired. As discussed in the introduction of this section, the motion of a space curve is determined up to rotations and translations by knowing how g, κ , and τ evolve. What is left to be determined are {W,U,V}, which is addressed in the next section.

7 Force Determination

7.1 Calculus of Variations

Our space curve is parameterized with respect to a general variable α. Using metric notation, one can define,

$$\frac{d}{ds} = \frac{1}{\sqrt{g}}\frac{d}{d\alpha}\,, \quad g^{\frac{1}{2}} = |r_\alpha|, \tag{19}$$

where the total contour length is,

$$S = \int_{\alpha_{min}}^{\alpha_{max}} g^{\frac{1}{2}}\, d\alpha. \tag{20}$$

The action, I, is defined as the path integral of the Lagrangian between two fixed end points. Written in integral form for a generic Lagrangian,

$$I = \int_{\alpha_{min}}^{\alpha_{max}} L(\alpha, \mathbf{r}, \mathbf{r}_\alpha, \mathbf{r}_{\alpha\alpha}, \mathbf{r}_{\alpha\alpha\alpha}) g^{\frac{1}{2}}\; d\alpha, \tag{21}$$

where the subscripts, $\{_\alpha, _{\alpha\alpha}, _{\alpha\alpha\alpha}\}$, signify differentiation with respect to α.

Using the principle of least action, one can derive the higher-order Euler equation needed to minimize the action with respect to some change in $\mathbf{r}(\alpha)$. The result, derived in the appendix

below, *Appendix A*, is the following:

$$\frac{\partial \hat{L}}{\partial \mathbf{r}} - \frac{d}{d\alpha}\left(\frac{\partial \hat{L}}{\partial \mathbf{r}_\alpha}\right) + \frac{d^2}{d\alpha^2}\left(\frac{\partial \hat{L}}{\partial \mathbf{r}_{\alpha\alpha}}\right) - \frac{d^3}{d\alpha^3}\left(\frac{\partial \hat{L}}{\partial \mathbf{r}_{\alpha\alpha\alpha}}\right) = \frac{\delta E}{\delta r}\,, \tag{22}$$

where $\hat{L} = L(\alpha, \mathbf{r}, \mathbf{r}_\alpha, \mathbf{r}_{\alpha\alpha}, \mathbf{r}_{\alpha\alpha\alpha})g^{\frac{1}{2}}$. This is a general conclusion which can be applied to any third-order Lagrangian written in terms of α. The next section uses this result to analyze the behavior of our specific system.

It is important to note that one can use *Equation 22* only in combination with a set of boundary conditions determined while minimizing the action. This is also derived and discussed in the appendix.

7.2 Curve-dependent force equations in 2D

Although correct and complete, applying *Equation 22* to a given Lagrangian is tedious and the calculations are prone to error. To facilitate this step for a Lagrangian with a curve-dependent energetic term, such as elastic energy, one can rewrite this equation in terms of κ and τ instead of α, $\mathbf{r}$, $\mathbf{r}_\alpha$, $\mathbf{r}_{\alpha\alpha}$ $\mathbf{r}_{\alpha\alpha\alpha}$ by using the chain rule, given,

$$\kappa = \frac{|r_\alpha \times \mathbf{r}_{\alpha\alpha}|}{(\mathbf{r}_\alpha \cdot \mathbf{r}_\alpha)^{\frac{1}{2}}}, \tag{23}$$

$$\tau = \frac{\mathbf{r}_\alpha \times \mathbf{r}_{\alpha\alpha} \cdot \mathbf{r}_{\alpha\alpha\alpha}}{|\mathbf{r}_\alpha \times \mathbf{r}_{\alpha\alpha}|^2}. \tag{24}$$

Let us first restrict ourselves to two dimensions, so that the Lagrangian has dependence only on κ and g. *Equation 22* rewritten using the chain rule for the two-dimensional case is,

$$-g^{-\frac{1}{2}}\frac{\delta E_e}{\delta \mathbf{r}} = -g^{-\frac{1}{2}}\left[\frac{\partial\left(L(\kappa,g)\ g^{\frac{1}{2}}\right)}{\partial \mathbf{r}} - \frac{d}{d\alpha}\left(\frac{\partial\left(L(\kappa,g)\ g^{\frac{1}{2}}\right)}{\partial \mathbf{r}_\alpha}\right) + \frac{d^2}{d\alpha^2}\left(\frac{\partial\left(L(\kappa,g)\ g^{\frac{1}{2}}\right)}{\partial \mathbf{r}_{\alpha\alpha}}\right)\right], \tag{25}$$

$$-g^{-\frac{1}{2}}\frac{\delta E_e}{\delta \mathbf{r}} = -g^{-\frac{1}{2}}\left[-\frac{d}{d\alpha}\left(g^{\frac{1}{2}}\frac{\partial L(\kappa,g)}{\partial \kappa}\frac{\partial \kappa}{\partial \mathbf{r}_\alpha} + 2g\frac{\partial L(\kappa,g)}{\partial g}\ \hat{\mathbf{t}} + L(\kappa,g)\ \hat{\mathbf{t}}\right) + \frac{d^2}{d\alpha^2}\left(g^{\frac{1}{2}}\frac{\partial L(\kappa,g)}{\partial \kappa}\frac{\partial \kappa}{\mathbf{r}_{\alpha\alpha}}\right)\right], \tag{26}$$

where the subscript $\{_e\}$ refers to the elastic energy term.

We have assumed here that there is no spatial dependence. Using *Equation 26*, one also needs the following:

$$\frac{\partial \kappa}{\partial \mathbf{r}_\alpha} = -\kappa g^{-\frac{1}{2}}\,\hat{\mathbf{t}} - \frac{1}{2}\,g^{-\frac{3}{2}}\,g_\alpha \hat{\mathbf{n}}, \tag{27}$$

$$\frac{\partial \kappa}{\partial \mathbf{r}_{\alpha\alpha}} = g^{-\frac{1}{2}}\,\hat{\mathbf{n}}. \tag{28}$$

These relationships were derived by using *Equations 23* and ploughing through the differentiation. By inserting them directly into *Equation 26*, we have derived general equations for the force components in 2D. The tangential and normal components are the following:

$$Wo = a\left[\frac{1}{2}\,g^{-\frac{3}{2}}\,g_\alpha \kappa \frac{\partial L}{\partial \kappa} + 2g^{-\frac{1}{2}}\,g_\alpha \frac{\partial L}{\partial g} + g^{-\frac{1}{2}}\,\kappa \frac{d}{d\alpha}\left(\frac{\partial L}{\partial \kappa}\right) + 2g^{\frac{1}{2}}\,\frac{d}{d\alpha}\left(\frac{\partial L}{\partial g}\right) + g^{-\frac{1}{2}}\,\frac{\partial L}{\partial \alpha}\right], \tag{29}$$

$$Uo = a\left[\frac{1}{2}\,g^{-\frac{5}{2}}\,g_\alpha^2 \kappa \frac{\partial L}{\partial \kappa} - \frac{1}{2}\,g_{\alpha\alpha}\partial_\kappa L - \frac{1}{2}\,g^{-\frac{3}{2}}\,g_\alpha \frac{d}{d\alpha}\left(\frac{\partial L}{\partial \kappa}\right) - g^{-\frac{1}{2}}\,\frac{d^2}{d^2\alpha}\left(\frac{\partial L}{\partial \kappa}\right) + 2g^{\frac{1}{2}}\,\kappa\left(\frac{\partial L}{\partial g}\right) + g^{-\frac{1}{2}}\,\kappa L\right]. \tag{30}$$

These will be used in case studies to follow.

7.2.1 Case study: 2D Elastic force, Interfacial growth model

Using the above definitions, geometric relations, and *Equation 29 and 30*, we now have the means to derive the elastic energy contribution to the equation of motion of an extensible, elastic curve. The curve in this case could represent an interface that expands due to forces dependent upon local curvature.

V, the elastic bending energy term of the Lagrangian ($L = T - V - C$) becomes,

$$L = -V(\alpha) = -\frac{1}{2}\,a\frac{\kappa^2}{g}, \tag{31}$$

where a is the elastic flexure. For our purposes, the flexure is constant along the length of the space curve. The normal component of the force due to the elastic energy is therefore,

$$U_e = a\left[-g^{-\frac{7}{2}}\,g_\alpha^2 \kappa + \frac{3}{2}\,g^{-\frac{5}{2}}\,g_\alpha \kappa_\alpha + \frac{1}{2}\,g^{-\frac{5}{2}}\,g_{\alpha\alpha}\kappa - g^{-\frac{3}{2}}\,\kappa_{\alpha\alpha} - \frac{1}{2}\,g^{-\frac{3}{2}}\,\kappa^3\right], \tag{32}$$

$$W_e = 0, \tag{33}$$

where the subscript $\{_e\}$ refers to the elastic force. When the curve is evolving solely under the influence of elastic energy, the unconstrained evolution equations for both κ and g are

determined now that U_e and W_e are known.

$$\zeta \dot{g} = -2g^{\frac{1}{2}}\,\kappa U_e \tag{34}$$

$$\zeta \dot{\kappa} = -\frac{1}{2}\,g_\alpha g^{-\frac{3}{2}}\,\partial_\alpha U_e + g^{-\frac{1}{2}}\,\partial_{\alpha\alpha} U_e \tag{35}$$

For intuition, let us consider the example of a circle. The curvature is equal to $\tilde{\kappa} = 1/\mathrm{R}$, where R is the radius. In terms of α, the angular coordinate here, $\kappa = 1$ and $g^{\frac{1}{2}} = R$. The derivatives κ_α, $\kappa_{\alpha\alpha}$, g_α, etc., are equal to zero for this cylindrically symmetric case. Therefore the force components and the resulting evolution equation are the following:

$$\begin{aligned}
U_e &= -\frac{a}{2}\,g^{-\frac{3}{2}}\,\kappa^3 = -\frac{a}{2R^3}\,,\\
W_e &= 0,\\
\zeta \dot{g} &= -2g^{\frac{1}{2}}\,\kappa U_e = \frac{a}{R^2}\,,\\
\zeta \dot{\kappa} &= g^{-\frac{1}{2}}\,\partial_{\alpha\alpha}(U_e) = 0.
\end{aligned} \tag{36}$$

The space curve in the shape of a circle, evolving under the influence of its own curvature is therefore expanding at a rate determined by $\dot{g}$. This is the behavior one would expect, since by doing so, the curve is reducing its elastic energy.

7.2.2 Case study: 2D Elastic and random forces, Tumor growth model

Tumors have been found to follow Mullins-Herring growth (MH) [40, 41]. MH is a part of a universality class, which describes the dynamics of an elastic interface in a 2D environment of noise. The elastic interface in this case is the curve that defines the edge of the tumor, and the noise represents the collective effect of various biological processes.

The framework developed thus far can in principle accommodate the addition of random forces to treat this particular case [42]. The forces due to interfacial elasticity are given by *Equation 32* and *33*. Added to that is the random force, with which the resulting equation reads,

$$\zeta \dot{\mathbf{r}}\,dt = \left(W\hat{\mathbf{t}} + U\hat{\mathbf{n}} + V\hat{\mathbf{b}}\right)\,dt = (Wo\,dt + \sigma_t dB_t)\,\hat{\mathbf{t}} + (Uo\,dt + \sigma_n dB_n)\,\hat{\mathbf{n}} + (Vo\,dt + \sigma_b dB_b)\,\hat{\mathbf{b}}, \tag{37}$$

where B represents a stocastic, random variable (Weiner) and σ represents the standard deviation of the noise. The equation for the metric is,

$$\zeta \dot{g}\ dt = -2g^{\frac{1}{2}}\,\kappa U\ dt = -2g^{\frac{1}{2}}\,\kappa\left(U_e\ dt + \sigma_n dB_n\right). \tag{38}$$

We are currently investigating this application [42].

7.3 Curve-dependent force equations in 3D

The three dimensional case is naturally much more cumbersome. Starting from *Equation 22* again and rewriting for a Lagrangian in 3D, L(τ,κ,g),

$$-g^{-\frac{1}{2}}\frac{\delta E_e}{\delta \mathbf{r}} = -g^{-\frac{1}{2}}\left[-\frac{d}{d\alpha}\left(g^{\frac{1}{2}}\left(\frac{\partial L}{\partial \kappa}\frac{\partial \kappa}{\partial \mathbf{r}_\alpha} + \frac{\partial L}{\partial \tau}\frac{\partial \tau}{\partial \mathbf{r}_\alpha}\right) + \left(2g\frac{\partial L}{\partial g} + L\right)\hat{\mathbf{t}}\right) + \frac{d^2}{d\alpha^2}\left(g^{\frac{1}{2}}\left(\frac{\partial L}{\partial \kappa}\frac{\partial \kappa}{\mathbf{r}_{\alpha\alpha}} + \frac{\partial L}{\partial \tau}\frac{\partial \tau}{\mathbf{r}_{\alpha\alpha}}\right)\right) - \frac{d^3}{d\alpha^3}\left(g^{\frac{1}{2}}\frac{\partial L}{\partial \tau}\frac{\partial \tau}{\mathbf{r}_{\alpha\alpha\alpha}}\right)\right]. \tag{39}$$

The remaining definitions that one needs are,

$$\frac{\partial \tau}{\partial \mathbf{r}_\alpha} = \tau\left(1 - 2g^{\frac{1}{2}} - \frac{g_\alpha^2}{2g\kappa^2}\left(g^{\frac{1}{2}} + \frac{1}{2}\right)\right)\hat{\mathbf{t}} + \frac{\tau g_\alpha}{2g\kappa}\hat{\mathbf{n}} + \frac{1}{2}\left(\frac{\kappa_\alpha g_\alpha}{g\kappa^2} - \frac{g_{\alpha\alpha}}{g\kappa} + 2\kappa + \frac{3g_\alpha^2}{2g^2\kappa}\right)\hat{\mathbf{b}}, \tag{40}$$

$$\frac{\partial \tau}{\partial \mathbf{r}_{\alpha\alpha}} = \frac{\tau g_\alpha}{2g^{\frac{1}{2}}\kappa^2}\hat{\mathbf{t}} + \tau\left(\frac{1 - g^{\frac{1}{2}}}{\kappa}\right)\hat{\mathbf{n}} + \left(-\frac{g_\alpha}{g\kappa} - \frac{\kappa_\alpha}{\kappa^2}\right)\hat{\mathbf{b}}, \tag{41}$$

$$\frac{\partial \tau}{\partial \mathbf{r}_{\alpha\alpha\alpha}} = \frac{1}{\kappa}\hat{\mathbf{t}}. \tag{42}$$

Now the resultant force components in terms of a general Lagrangian in three dimensions can be determined. The complexity of the resulting equations encourages one to reevaluate their usefulness, and for this reason they are excluded.

8 Length Constraint

In this report we set out to model polymers using space curve dynamics. Our curves thus far are lacking one important property that is imperative for our intended application: constant length. Although stretchable to some extent, the carbon-carbon and other bonds forming the backbone of polymer chains are effectively rigid, resulting in both global and local inextensibility. One can incorporate a Lagrange multiplier to provide a fictitious force acting to maintain a conserved geometric quantity such as length.

8.1 Updated equation of motion

Adding a term to our Lagrangian from above, *Equation 31*, we have (L = T - V - C),

$$L = -V - C = -\frac{1}{2}\, a\frac{\kappa^2}{g} - \lambda, \tag{43}$$

where $\lambda(\alpha)$ is the fictitious force imposing the length constraint. Minimizing the action, but leaving the elastic forces in general terms, we get the following equations, where U_o and W_o are the force components from all other forces.

$$U = U_o - g^{-\frac{1}{2}}\,\kappa\lambda \tag{44}$$

$$W = W_o - g^{-\frac{1}{2}}\,\lambda_\alpha \tag{45}$$

Local inextensibility requires that $\partial_t\ (\hat{\mathbf{t}} \cdot \hat{\mathbf{t}}) = 0$, requiring that $\hat{\mathbf{t}}$ remains normalized and that the metric does not evolve. Applying this to *Equation 6* and using the Serret-Frenet relations, we conclude that

$$\partial_\alpha W = \kappa U. \tag{46}$$

This is the condition which needs to be satisfied in order for our space curve to maintain constant length. Plugging in *Equation 44* and *Equation 45* into this equation, we arrive at a partial differential equation which can be solved numerically for lambda, our fictitious forces.

$$g^{-\frac{1}{2}}\,\lambda_{\alpha\alpha} - \frac{1}{2}\,g^{-\frac{3}{2}}\,g_\alpha\lambda_\alpha - \kappa^2 g^{-\frac{1}{2}}\,\lambda = \partial_\alpha W_o - \kappa U_o. \tag{47}$$

8.2 Case study: 2D Elastic dynamics

For the specific case of a two-dimensional curve of constant length evolving under its own curvature, one can now determine the evolution equation for kappa. The general equation from above is,

$$\zeta\partial_t\kappa = -\frac{1}{2}\,g_\alpha g^{-\frac{3}{2}}\,(U_\alpha + \kappa W) + g^{-\frac{1}{2}}\,(U_{\alpha\alpha} + \kappa W_\alpha + \kappa_\alpha W). \tag{48}$$

After substituting for W_α using *Equation 46*, it can then be rewritten as,

$$\zeta\partial_t\kappa = -\frac{1}{2}\,g_\alpha g^{-\frac{3}{2}}\,(U_\alpha + \kappa W) + g^{-\frac{1}{2}}\,(U_{\alpha\alpha} + \kappa^2 U + \kappa_\alpha W). \tag{49}$$

The metric evolution equation is,

$$\zeta \dot{g} = 2g^{\frac{1}{2}} \left(W_\alpha - \kappa U\right) = 0. \tag{50}$$

In the case of unconstrained motion, two evolution equations were needed, one for the metric and one for κ. Because here length is being conserved, the number of evolution equations should be reduced by the number of conserved quantities, as we observe above. For simplicity, we can work in terms of contour length and evolve $\tilde{\kappa}$, the real curvature. The evolution equation and normal and tangential elastic forces are then

$$\zeta \partial_t \tilde{\kappa} = U'' + \tilde{\kappa}^2 U + \tilde{\kappa}' W, \tag{51}$$

$$U_e = a\left(\kappa'' + \frac{1}{2}\kappa^3\right), \tag{52}$$

$$W_e = 0. \tag{53}$$

9 Extension to 3D: Hasimoto Transformation

Thus far we have only looked at case studies of curves in two dimensions. In the three-dimensional case, one would need to evolve the curvature, torsion, and metric according to the equations derived in *Section 2* above, rewritten here:

$$\zeta \dot{\kappa} = -\frac{1}{2} g_\alpha g^{-\frac{3}{2}} \left(U_\alpha + W\kappa - \tau V\right) + g^{-\frac{1}{2}} \left(U_{\alpha\alpha} + \kappa W_\alpha + \kappa_\alpha W - 2\tau V_\alpha - \tau_\alpha V + \tau^2 U\right), \tag{54}$$

$$\zeta \dot{\tau} = \partial_\alpha \left[\frac{1}{\kappa}\left[-\frac{1}{2} g_\alpha g^{-\frac{3}{2}} \left(V_\alpha + \tau U\right) + g^{-\frac{1}{2}} \left(V_{\alpha\alpha} + 2\tau U_\alpha + \tau_\alpha U + \tau\kappa W - \tau^2 V\right)\right]\right] + g^{-\frac{1}{2}} \left(\kappa V_\alpha + \kappa\tau U\right), \tag{55}$$

$$\zeta \dot{g} = 2g^{\frac{1}{2}} \left(W_\alpha - \kappa U\right). \tag{56}$$

The equation for torsion is extremely complicated, not to mention singular at points where the curvature is equal to zero. We can simplify the three-dimensional dynamics by recasting the formalism using complex variables and rederiving the evolution equations. By implementing the so-called Hasimoto transformation, the time evolution is reduced to solving two evolution equations: one for the newly-defined complex curvature and one for the metric.

9.1 General formulation

Following from Hasimoto's seminal paper [43], we first write,

$$\partial_\alpha \left(\hat{\mathbf{n}} + i\hat{\mathbf{b}}\right) = -i\tau \left(\hat{\mathbf{n}} + i\hat{\mathbf{b}}\right) - \kappa\hat{\mathbf{t}}, \tag{57}$$

which prompts the definition of new variables $\mathbf{N}$, ψ, and ϕ.

$$\mathbf{N} = \left(\hat{\mathbf{n}} + i\hat{\mathbf{b}}\right) e^{i\phi} \tag{58}$$

$$\psi = \kappa\ e^{i\phi} \tag{59}$$

$$\phi = \int_{\alpha_{min}}^{\alpha_{max}} \tau\ g^{\frac{1}{2}}\ d\alpha \tag{60}$$

The new variable ψ can be thought of as a complex curvature, and ϕ can be viewed as either an integrating factor or a phase angle associated with the new complex basis vector $\mathbf{N}$. Using the Serret-Frenet relations and the new variables, we can rewrite the complex Serret-Frenet relations as,

$$\partial_\alpha \mathbf{N} = -\psi\hat{\mathbf{t}}, \tag{61}$$

and

$$\partial_\alpha \hat{\mathbf{t}} = Re\left[\psi\bar{\mathbf{N}}\right] = \frac{1}{2}\left(\bar{\psi}\mathbf{N} + \psi\bar{\mathbf{N}}\right), \tag{62}$$

where the bar signifies complex conjugation. The orthogonality relations between $\hat{\mathbf{t}}$, $\mathbf{N}$, and $\bar{\mathbf{N}}$ are,

$$\hat{\mathbf{t}}\cdot\hat{\mathbf{t}} = 1 \qquad \mathbf{N}\cdot\bar{\mathbf{N}} = 2 \qquad \mathbf{N}\cdot\mathbf{N} = 0 \qquad \mathbf{N}\cdot\hat{\mathbf{t}} = 0,\ etc. \tag{63}$$

The goal is to determine an evolution equation for the new complex curvature, ψ, as we did for κ and τ above. Recalling the procedure to do so, we need to assume the compatibility of partial derivatives and match each basis component.

9.1.1 Determination of $\dot{g}$ and $\dot{\hat{\mathbf{t}}}$

Let us first define the resolved force components, as we did in *Equation 6* above.

$$\zeta\dot{\mathbf{r}} = Y\hat{\mathbf{t}} + \bar{Z}\mathbf{N} + Z\bar{\mathbf{N}} \tag{64}$$

The coefficients {Y,Z} exist in the complex set. They are related to {W,U,V} by the following equations,

$$Y = W, \tag{65}$$

$$Z = \frac{1}{2}\left(U + iV\right)e^{i\phi}. \tag{66}$$

The evolution of the metric and the tangent vector can be determined by differentiation:

$$\partial_\alpha(\zeta\dot{\mathbf{r}}) = \zeta\partial_t(g^{\frac{1}{2}}\hat{\mathbf{t}}) = \left(Y_\alpha - \psi\bar{Z} - \bar{\psi}Z\right)\hat{\mathbf{t}} + \left(\frac{1}{2}\bar{\psi}Y + \bar{Z}_\alpha\right)\mathbf{N} + \left(\frac{1}{2}\psi Y + Z_\alpha\right)\bar{\mathbf{N}}, \tag{67}$$

leading to,

$$\zeta\dot{g} = 2g^{\frac{1}{2}}\left(Y_\alpha - \psi\bar{Z} - \bar{\psi}Z\right), \tag{68}$$

$$\zeta\dot{\hat{\mathbf{t}}} = g^{-\frac{1}{2}}\left[\left(\frac{1}{2}\bar{\psi}Y + \bar{Z}_\alpha\right)\mathbf{N} + \left(\frac{1}{2}\psi Y + Z_\alpha\right)\bar{\mathbf{N}}\right]. \tag{69}$$

9.1.2 Determination of $\dot{\mathbf{N}}$ and $\dot{\psi}$

The evolution of $\mathbf{N}$ can be written as,

$$\zeta\dot{\mathbf{N}} = \alpha\mathbf{N} + \beta\bar{\mathbf{N}} + \gamma\hat{\mathbf{t}}. \tag{70}$$

Using the orthogonality conditions (*Equation 63*), $\dot{\hat{\mathbf{t}}}$ (*Equation 69*), and the above (*Equation 70*), the coefficients α, β, and γ are determined.

$$\zeta\partial_t(\bar{\mathbf{N}}\cdot\mathbf{N}) = 0, \qquad (\zeta\dot{\bar{\mathbf{N}}})\cdot\mathbf{N} + \bar{\mathbf{N}}\cdot(\zeta\dot{\mathbf{N}}) = 2\bar{\alpha} + 2\alpha, \qquad \alpha = iR \tag{71}$$

$$\zeta\partial_t(\bar{\mathbf{N}}\cdot\bar{\mathbf{N}}) = 0, \qquad (\zeta\dot{\bar{\mathbf{N}}})\cdot\bar{\mathbf{N}} + \bar{\mathbf{N}}\cdot(\zeta\dot{\bar{\mathbf{N}}}) = 2\bar{\beta} + 2\bar{\beta}, \qquad \beta = 0 \tag{72}$$

$$\zeta\partial_t(\mathbf{N}\cdot\hat{\mathbf{t}}) = 0, \qquad (\zeta\dot{\mathbf{N}})\cdot\hat{\mathbf{t}} + \mathbf{N}\cdot(\zeta\dot{\hat{\mathbf{t}}}) = \gamma + 2g^{-\frac{1}{2}}(\frac{1}{2}\psi Y + Z_\alpha), \qquad \gamma = -g^{-\frac{1}{2}}\left(\psi Y + 2Z_\alpha\right) \tag{73}$$

$$\zeta\dot{\mathbf{N}} = iR\mathbf{N} - g^{-\frac{1}{2}}\left(\psi Y + 2Z_\alpha\right)\hat{\mathbf{t}} \tag{74}$$

R is a real number. One can now compare the components of the temporal derivative of *Equation 61* and the derivative with respect to α of *Equation 74*.

$$\begin{aligned}\zeta\partial_\alpha\dot{\mathbf{N}} = &-\left(iR\psi + g^{-\frac{1}{2}}\left(\partial_\alpha\left(\psi Y\right) + 2Z_{\alpha\alpha}\right) - \frac{1}{2}g^{-\frac{3}{2}}g_\alpha\left(\psi Y + 2Z_\alpha\right)\right)\hat{\mathbf{t}} + \\ &\left(iR_\alpha - \frac{1}{2}g^{-\frac{1}{2}}\bar{\psi}\left(\psi Y + 2Z_\alpha\right)\right)\mathbf{N} - \frac{1}{2}g^{-\frac{1}{2}}\psi\left(\psi Y + 2Z_\alpha\right)\bar{\mathbf{N}}\end{aligned} \tag{75}$$

$$\zeta\partial_t\mathbf{N}_\alpha = -\left(\zeta\dot{\psi}\hat{\mathbf{t}} + \psi(\zeta\dot{\hat{\mathbf{t}}})\right) = -\zeta\dot{\psi}\hat{\mathbf{t}} - \psi\ g^{-\frac{1}{2}}\left[\left(\frac{1}{2}\bar{\psi}Y + \bar{Z}_\alpha\right)\mathbf{N} - \left(\frac{1}{2}\psi Y + Z_\alpha\right)\bar{\mathbf{N}}\right] \tag{76}$$

Matching the $\hat{\mathbf{t}}$ components, we get,

$$\zeta\dot{\psi} = iR\psi + g^{-\frac{1}{2}}\left(\partial_\alpha\left(\psi Y\right) + 2Z_{\alpha\alpha}\right) - \frac{1}{2}g^{-\frac{3}{2}}g_\alpha\left(\psi Y + 2Z_\alpha\right). \tag{77}$$

The $\mathbf{N}$ components yield,

$$R_\alpha = -ig^{-\frac{1}{2}}\left(\bar{\psi}Z_\alpha - \psi\bar{Z}_\alpha\right) = 2Im\left[\bar{\psi}Z_\alpha\right]. \tag{78}$$

We can integrate *Equation 78* to find R, in the process defining a time-dependent integrating factor A(t).

$$R = 2\left(\int^\alpha g^{\frac{1}{2}}\ Im\left[\bar{\psi}Z_\alpha\right]d\alpha + A(t)\right) = 2\left(Im\left[Z\bar{\psi}\right] - \int^\alpha g^{\frac{1}{2}}\ Im\left[Z\bar{\psi}_\alpha\right]d\alpha + A(t)\right) \tag{79}$$

The evolution equation is now,

$$\zeta\dot{\psi} = 2i\psi\left(Im\left[Z\bar{\psi}\right] - \int^\alpha g^{\frac{1}{2}}\ Im\left[Z\bar{\psi}_\alpha\right]d\alpha + A(t)\right) + g^{-\frac{1}{2}}\left(\partial_\alpha\left(\psi Y\right) + 2Z_{\alpha\alpha}\right) - \frac{1}{2}g^{-\frac{3}{2}}g_\alpha\left(\psi Y + 2Z_\alpha\right). \tag{80}$$

The integrating factor, A(t), can be eliminated by a redefinition of variables.

$$\Psi = \psi e^{-2i\int_0^t A(t)\ dt}. \tag{81}$$

A(t) represents a shift in the origin of the phase of $\mathbf{N}$. A(t) will be set equal to zero from here onward without loss of generality. Our final result is,

$$\zeta\dot{\psi} = 2i\psi\left(Im\left[Z\bar{\psi}\right] - \int^\alpha g^{\frac{1}{2}}\ Im\left[Z\bar{\psi}_\alpha\right]d\alpha\right) + g^{-\frac{1}{2}}\left(\partial_\alpha\left(\psi Y\right) + 2Z_{\alpha\alpha}\right) - \frac{1}{2}g^{-\frac{3}{2}}g_\alpha\left(\psi Y + 2Z_\alpha\right). \tag{82}$$

Our results are completely general and can accommodate growth through a changing metric.

9.2 Length constraint

If one wishes to model a polymer chain, the geometric constraint of inextensibility can be incorporated, as it was above, by requiring $\zeta\dot{g}$ to be zero. We can rewrite our equations in terms of contour length, s, the spatial derivatives as $\{',''\}$, and the real curvature ($\tilde{\kappa}$) and torsion ($\tilde{\tau}$). The initial definitions become:

$$\mathbf{N} = \left(\hat{\mathbf{n}} + i\hat{\mathbf{b}}\right)e^{i\phi} \tag{83}$$

$$\psi = \tilde{\kappa}\ e^{i\phi} \tag{84}$$

$$\phi = \int_0^s \tilde{\tau}\ ds \tag{85}$$

$$\mathbf{N}' = -\psi\hat{\mathbf{t}} \tag{86}$$

$$\hat{\mathbf{t}}' = Re\left[\psi\bar{\mathbf{N}}\right] = \frac{1}{2}\left(\bar{\psi}\mathbf{N} + \psi\bar{\mathbf{N}}\right) \tag{87}$$

The inextensibility requirement is:

$$Y' = \psi\bar{Z} + \bar{\psi}Z = 2Re\left[\psi\bar{Z}\right]. \tag{88}$$

In terms of the real force components, we recover the familiar result,

$$W' = \tilde{\kappa}U. \tag{89}$$

The integrating factor, R, becomes:

$$R = 2\left(Im\left[Z\bar{\psi}\right] - \int^s Im\left[Z\bar{\psi}'\right]\right). \tag{90}$$

The resultant evolution equations are:

$$\zeta\dot{\hat{\mathbf{t}}} = \left(\frac{1}{2}\bar{\psi}Y + \bar{Z}'\right)\mathbf{N} + \left(\frac{1}{2}\psi Y + Z'\right)\bar{\mathbf{N}}, \tag{91}$$

$$\zeta\dot{\mathbf{N}} = iR\mathbf{N} - \left(2Z' + \psi Y\right)\hat{\mathbf{t}}, \tag{92}$$

$$\zeta\dot{\psi} = 2i\psi\left(Im\left[Z\bar{\psi}\right] - \int^s Im\left[Z\bar{\psi}'\right]\right) + 2Z'' + \left(\psi Y\right)'. \tag{93}$$

9.2.1 Case study: 3D Elastic dynamics

The result, *Equation 93*, differs from the result published by Goldstein and Langer for the Lagrangian, $L = -\frac{a}{2}\tilde{\kappa}^2 - \lambda$, corresponding to elastic dynamics [36]. Their result, using the definition $\Gamma = 2Z$ and the real components of force, {W,U,V}, is,

$$\zeta\dot{\psi} = \left(\partial_{ss} + |\psi|^2\right)\Gamma + \psi\ \int^s ds'\ Im\left[\psi'\bar{\Gamma}\right] + \psi' W. \tag{94}$$

Ours, rewritten with equivalent definitions and format, is,

$$\zeta\dot{\psi} = \left(\partial_{ss} + |\psi|^2\right)\Gamma + i\psi\int^s ds'\ Im\left[\psi'\bar{\Gamma}\right] + \psi' W. \tag{95}$$

The discrepancy that has not yet been reconciled is an i in the second term. I am going to write this off as a typo, given that our result does agree with [44]

10 Numerical Implementation

10.1 Algorithm

One can use the following algorithm to implement 3D dissipative curve dynamics utilizing the Hasimoto transformation.

1. Take a discrete set of points that represent the curve, equally spaced in terms of contour length, s, and determine κ(s) and τ(s). This is the initial configuration.

2. From this initial configuration:

   a. Integrate τ to determine ϕ, according to *Equation 60*.

   b. Construct ψ from *Equation 59*.

3. Once ψ has been constructed, begin the iterative loop.

   a. Calculate ψ', ψ'', ψ''''.

   b. Determine κ and κ'' from the above, from which λ and λ' can be calculated.

   c. Calculate Γ.

   d. Calculate the right-hand side of *Equation 82*.

   e. Integrate ψ a single time step using Euler integration, and continue from *3.a* above.

10.2 Preliminary results

Issues arise when taking high order derivatives, namely in the calculation of ψ''''. Standard finite difference schemes are notoriously numerically unstable for most choices of timesteps. Psuedospectral methods can allieviate these difficults by dealing with the derivatives of the linear parts in Fourier space [45].

A code has been developed which implements the algorithm above for the case of 3D elastic dynamics. Preliminary results are shown in the images located at the end of the report. *Figure 1* shows the relaxation of a closed, bent curve into the lowest energy configuration of a circle. *Figure 2* and *Figure 3* are plots of the real and imaginary components of the complex curvature ψ, and *Figure 4* is the real curvature, $\tilde{\kappa}$. For this simple case study the results are as one would predict.

One difficulty quickly becomes evident while working in terms of a body coordinate for examples of closed curves. In real space representations, the errors in the calculated trajectories

of atoms and molecules collectively diverge from the true evolution over a period of time. We would expect the same for our variable, ψ, after multiple time steps. The reconstructed curve at the end of the simulation does not then close, however, as we could not reasonably expect the error in the curvature and the torsion that accumulates to cancel out. This problem can be dealt with by implementing a periodic adjustment to the values of ψ. I am currently developing a (hopefully) clever scheme to do so. Once we have attained greater confidence in the real-space representation, a simple Lennard-Jones interaction can easily be added.

11 Discrete Counterpart

A discretized counterpart to the continuous curve dynamics is concurrently being considered which could serve either as a benchmark for or an alternative to the continuous case. In this model, the continuously curved wire is replaced with a sequence of straight segments of length l. The straight segments are connected at the ends, forming nodes. The mass of the wire is understood to be concentrated at the nodes, where the localized mass is then given by $m = \rho\ l$. The constant ρ is the mass density of the wire. The elastic bending energy integral of the continuous wire is now replaced by a discrete sum. The variable θ_i is the angular deviation from a straight line of adjacent segments meeting at the i'th node. The nodes, in addition to being the location of the concentrated mass, are also where the Lennard-Jones interactions between segments of the filament are assumed to be concentrated. The discrete model replaces the continuous one in this way.

A functional code has already been developed. Rattle, an algorithm used to integrate equations of motion with internal constraints, is used to evolve the polymer in time [46]. A simple bending energy has been used to calculate the force on the curve,

$$E_{elastic} = \frac{a\ l}{2} \sum \theta_i^2. \tag{96}$$

The elastic force is simply the gradient of *Equation 96*. In order to simulate a solution or melt environment, temperature is maintained through the addition of a Langevin force term. A Lennard-Jones interaction is also incorporated into the force calculation. Inertial forces can be present or damped. Together these encapsulate the environment and conservative forces experienced by Kratky worm-like chain.

For the case of just elastic bending energy in a dissipative regime, analogous to that of the results shown for the continuous example, the preliminary results look very promising. The relaxation of the curvature is shown in *Figure 5*. The shape relaxation is qualitatively equivalent to *Figure 1*.

12 Beyond the Serret-Frenet Relations

The entire work presented here has been developed within the framework of the Serret-Frenet relations. Naturally, there are limitations one must consider. We have taken a space curve, overlain it with an elastic filament, and declared that the motion of this space curve represents the dynamics of the physical object; however, the filament has some finite cross section which we are neglecting. In the present formulation, the minimum energy configuration of a filament with an elliptical cross-section, for instance, is a configuration where the backbone follows a straight line. This configuration is irrespective of cross-sectional orientation, so a flat filament or one twisted about its backbone has the same energy.

As discussed in 4.1, κ and τ can be determined completely by information about the underlying space curve, and include no information about object orientation. The matrix representation in terms of contour length, s, is

$$\frac{\partial}{\partial s}\begin{pmatrix}\hat{\mathbf{t}}\\ \hat{\mathbf{n}}\\ \hat{\mathbf{b}}\end{pmatrix} = \begin{pmatrix}0 & \tilde{\kappa} & 0\\ -\tilde{\kappa} & 0 & \tilde{\tau}\\ 0 & -\tilde{\tau} & 0\end{pmatrix}\begin{pmatrix}\hat{\mathbf{t}}\\ \hat{\mathbf{n}}\\ \hat{\mathbf{b}}\end{pmatrix}. \tag{97}$$

It is possible to develop a framework that takes into account the object orientation with respect to the underlying space curve. To do so, the third component of the skew-symmetric matrix must be non-zero. In terms of a defined orthonormal frame,

$$\frac{\partial}{\partial s}\begin{pmatrix}\hat{\mathbf{e}}_1\\ \hat{\mathbf{e}}_2\\ \hat{\mathbf{e}}_3\end{pmatrix} = \begin{pmatrix}0 & \sigma_3 & -\sigma_2\\ -\sigma_3 & 0 & \sigma_1\\ \sigma_2 & -\sigma_1 & 0\end{pmatrix}\begin{pmatrix}\hat{\mathbf{e}}_1\\ \hat{\mathbf{e}}_2\\ \hat{\mathbf{e}}_3\end{pmatrix}. \tag{98}$$

The first unit vector, $\hat{\mathbf{e}}_\mathbf{1}$, is defined equivalently to $\hat{\mathbf{t}}$. Whereas before the second unit vector was represented by $\hat{\mathbf{n}}$ and pointed in the direction of the second derivative, here problems arise

because $\hat{\mathbf{n}}$ is not well defined in areas where the curvature is equal to zero. The basis vector $\hat{\mathbf{e}}_\mathbf{2}$ can instead indicate the material orientation, such as the normal to the flat side of a ribbon-like filament. The third vector, $\hat{\mathbf{e}}_\mathbf{3}$, is then the cross product of the preceding two.

The new matrix component σ_2 is often described as the "twist density", because of its role as effectively keeping track of how much the object is twisted about its backbone. Just as we have associated an energy to κ and τ above, we can now associate an energy to the values of σ_1, σ_2, and σ_3. The elastic energy up to quadratic order of an isotropic elastic filament is then,

$$E_{elastic} = \frac{a}{2} \int \left(\sigma_1^2 + \sigma_3^2\right)\ ds\ +\ \frac{b}{2} \int \sigma_2^2\ ds, \tag{99}$$

where the new constant b is the elastic constant associated with twisting [37].

The twist component, σ_2, has been excluded in this study for a few reasons. First, because of computational efficiency. Naturally, the inclusion of this additional energetic component incurs additional computational expense, and every calculation in an iterative procedure counts if one is hoping to model a large system of many polymer chains over extremely long timescales. It is no good, however, to have a very efficient code that is not accurately modeling the system you are attempting to study. The second reason the twist component has been excluded is because in this simple model we are assuming that the flexure, a, is much greater than the twist constant, b. The resultant forces from twist could therefore neglected. Whether this is a reasonable approximation has yet to be determined.

13 Present Conclusions and Future Plans

We have outlined the theoretical developments of curve dynamics for a computationally tractable model that treats polymer molecules as elastic filaments. Both continuous and discrete cases were considered. These results form the foundation for two primary objectives.

For our first objective, we must include a simple Lennard-Jones potential to represent interactions and a Langevin term to simulate a heat-bath. With interactions and temperature defined, we will be able to calculate a "stability diagram", similar to a phase diagram, which could be used to investigate the development of order through crystallization. For instance, at a high enough temperature, one would expect the interaction forces to be negligible compared to the stocastic forces, and the polymer would be amorphous. Upon cooling, it can minimize

its potential energy by crystallizing into possibly a helix or folded-chain structure. The degree of order can be quantified by the average radial distribution function of a polymer segment. A higher flexure corresponds to a higher persistence length, which could prohibit the formation of folds. The applications are most relevant to biological processes, not necessarily mechanical properties, but we see this as a feasible intermediate step in our investigations.

The remaining, primary goal is to model the elastic and plastic deformation of a real polymer system. Our intent is to study an entangled, linear chained polymers and also eventually a system which is cross-linked. Bulk properties will be confirmed, but a particular focus will be placed on investigating interfacial behavior, as discussed in the introduction.

For the first part of the project, we will follow a dual approach, using both the continuous curve dynamics and the discrete analog. We expect the discrete version to be more computationally viable and therefore more appropriate for the long simulations studying plastic deformation, part two of the project.

A Higher Order Euler Equation

The action, I, is defined as the path integral of the Lagrangian between two fixed end points. Written in integral form for a generic Lagrangian, L,

$$I = \int_{u_i}^{u_f} L(u, \mathbf{r}, \mathbf{r}', \mathbf{r}'')du, \tag{100}$$

where the single and double quotes, $\{',''\}$, signify differentiation with respect to u, to first and second order respectively.

It is worthwhile to note that the action is typically defined as an integral over space and time. However, I have excluded the time dependence here for purposes of clarity, knowing beforehand that the Lagrangian considered below has no $\dot{\mathbf{r}}$ dependence and will therefore produce no additional terms in our result.

The equation of motion of the chain is obtained by using the principle of least action. We rewrite the action in terms of the correct $\mathbf{r}$(u) plus some perturbation, $\epsilon\mathbf{\Theta}$(u), and require the variation with respect to ϵ be zero at $\epsilon = 0$. This will allow us to find the configuration of

lowest energy. The new coordinates are,

$$\mathbf{R} = \mathbf{r} + \epsilon\mathbf{\Theta}(u), \tag{101}$$

$$\mathbf{R}' = \mathbf{r}' + \epsilon\mathbf{\Theta}'(u), \tag{102}$$

$$\mathbf{R}'' = \mathbf{r}'' + \epsilon\mathbf{\Theta}''(u). \tag{103}$$

Here we have introduced a function $\mathbf{\Theta}$(u). This function has a continuous second derivative and is zero at the endpoints, which physically means that the endpoints are fixed. No other constraints have been imposed at this time, leaving $\mathbf{\Theta}$ otherwise arbitrary. The action can now be redefined in terms of *Equations 101-103*.

$$I = \int_{u_i}^{u_f} L(u, \mathbf{R}, \mathbf{R}', \mathbf{R}'', \epsilon, \mathbf{\Theta})du \tag{104}$$

Differentiating the action beneath the integral sign with respect to ϵ we get

$$\frac{dI}{d\epsilon} = \int_{u_i}^{u_f} \frac{d}{d\epsilon} L(u, \mathbf{R}, \mathbf{R}', \mathbf{R}'', \epsilon, \mathbf{\Theta})du. \tag{105}$$

Using the chain rule, the expanded integrand is

$$\frac{d}{d\epsilon} L(u, \mathbf{R}, \mathbf{R}', \mathbf{R}'', \epsilon, \mathbf{\Theta}) = \frac{\partial L}{\partial \mathbf{R}} \frac{d\mathbf{R}}{d\epsilon} + \frac{\partial L}{\partial \mathbf{R}'} \frac{d\mathbf{R}'}{d\epsilon} + \frac{\partial L}{\partial \mathbf{R}''} \frac{d\mathbf{R}''}{d\epsilon}, \tag{106}$$

leading to

$$\frac{dI}{d\epsilon} = \int_{u_i}^{u_f} \left[\frac{\partial L}{\partial \mathbf{R}} \frac{d\mathbf{R}}{d\epsilon} + \frac{\partial L}{\partial \mathbf{R}'} \frac{d\mathbf{R}'}{d\epsilon} + \frac{\partial L}{\partial \mathbf{R}''} \frac{d\mathbf{R}''}{d\epsilon} \right] du. \tag{107}$$

Rewritten in terms of $\mathbf{\Theta}$,

$$\frac{dI}{d\epsilon} = \int_{u_i}^{u_f} \left[\frac{\partial L}{\partial \mathbf{R}} \mathbf{\Theta}(u) + \frac{\partial L}{\partial \mathbf{R}'} \mathbf{\Theta}'(u) + \frac{\partial L}{\partial \mathbf{R}''} \mathbf{\Theta}''(u) \right] du. \tag{108}$$

Integrating by parts and keeping only terms up to first order in ϵ, the second and third terms of the integral are, respectively,

$$\int_{u_i}^{u_f} \frac{\partial L}{\partial \mathbf{R}'} \mathbf{\Theta}'(u)du = \left(\frac{\partial L}{\partial \mathbf{R}'} \mathbf{\Theta}(u) \right) \Bigg|_{u_i}^{u_f} - \int_{u_i}^{u_f} \frac{d}{du} \left(\frac{\partial L}{\partial \mathbf{R}'} \right) \mathbf{\Theta}(u)du, \tag{109}$$

$$\int_{u_i}^{u_f} \frac{\partial L}{\partial \mathbf{R}''} \mathbf{\Theta}''(u)du = \left[\frac{\partial L}{\partial \mathbf{R}''} \mathbf{\Theta}'(u) - \frac{d}{du} \left(\frac{\partial L}{\partial \mathbf{R}''} \right) \mathbf{\Theta}(u) \right] \Bigg|_{u_i}^{u_f} + \int_{u_i}^{u_f} \frac{d^2}{d^2u} \left(\frac{\partial L}{\partial \mathbf{R}''} \right) \mathbf{\Theta}(u)du. \tag{110}$$

Combining terms we have

$$\frac{dI}{d\epsilon} = \left[\frac{\partial L}{\partial \mathbf{R}'}\,\mathbf{\Theta}(u) + \frac{\partial L}{\partial \mathbf{R}''}\,\mathbf{\Theta}'(u) - \frac{d}{du}\left(\frac{\partial L}{\partial \mathbf{R}''}\right)\mathbf{\Theta}(u)\right]\Bigg|_{u_i}^{u_f} + \int_{u_i}^{u_f}\left[\frac{\partial L}{\partial \mathbf{R}} - \frac{d}{du}\left(\frac{\partial L}{\partial \mathbf{R}'}\right) + \frac{d^2}{d^2u}\left(\frac{\partial L}{\partial \mathbf{R}''}\right)\right]\mathbf{\Theta}(u)du. \tag{111}$$

We want

$$\frac{d}{d\epsilon}\,I(\epsilon) = \left(\frac{dI}{d\epsilon}\right)\Bigg|_{\epsilon} = 0. \tag{112}$$

Therefore, evaluating *Equation 111* at $\epsilon = 0$, we find

$$\left[\frac{\partial L}{\partial \mathbf{r}'}\,\mathbf{\Theta}(u) + \frac{\partial L}{\partial \mathbf{r}''}\,\mathbf{\Theta}'(u) - \frac{d}{du}\left(\frac{\partial L}{\partial \mathbf{r}''}\right)\mathbf{\Theta}(u)\right]\Bigg|_{u_i}^{u_f} = 0 \tag{113}$$

and

$$\int_{u_i}^{u_f}\left[\frac{\partial L}{\partial \mathbf{r}} - \frac{d}{du}\left(\frac{\partial L}{\partial \mathbf{r}'}\right) + \frac{d^2}{d^2u}\left(\frac{\partial L}{\partial \mathbf{r}''}\right)\right]\mathbf{\Theta}(u)du = 0. \tag{114}$$

The boundary conditions are automatically satisfied for a closed curves, the focus of this report. Finally, *Equation 114* must hold for arbitrary $\mathbf{\Theta}$. Therefore, the higher-order Euler equation is,

$$\frac{\partial L}{\partial \mathbf{r}} - \frac{d}{du}\left(\frac{\partial L}{\partial \mathbf{r}'}\right) + \frac{d^2}{du^2}\left(\frac{\partial L}{\partial \mathbf{r}''}\right) = 0. \tag{115}$$

The final result is a general conclusion which can be applied to any second-order Lagrangian. One can apply the method used for this derivation to determine an Euler equation for an even higher order, such as L(u,$\mathbf{r}$,$\mathbf{r}'$,$\mathbf{r}''$,$\mathbf{r}'''$). For this case, the equations one must satisfy are,

$$\left[\left(\frac{\partial L}{\partial \mathbf{r}'} - \frac{d}{du}\left(\frac{\partial L}{\partial \mathbf{r}''}\right) + \frac{d^2}{du^2}\left(\frac{\partial L}{\partial \mathbf{r}'''}\right)\right)\mathbf{\Theta} + \left(\frac{\partial L}{\partial \mathbf{r}''} - \frac{d}{du}\left(\frac{\partial L}{\partial \mathbf{r}'''}\right)\right)\mathbf{\Theta}' + \frac{\partial L}{\partial \mathbf{r}'''}\,\mathbf{\Theta}''\right]\Bigg|_{u_i}^{u_f} = 0 \tag{116}$$

and

$$\frac{\partial L}{\partial \mathbf{r}} - \frac{d}{du}\left(\frac{\partial L}{\partial \mathbf{r}'}\right) + \frac{d^2}{du^2}\left(\frac{\partial L}{\partial \mathbf{r}''}\right) - \frac{d^3}{du^3}\left(\frac{\partial L}{\partial \mathbf{r}'''}\right) = 0. \tag{117}$$

References

[1] A. Bernanose, M. Comte, and P. Vouaux. J. Chim. Phys., 50(64), (1953).

[2] J.H. Burroughes, D.D.C. Bradley, A.R. Brown, R.N. Marks, K. Mackay, R.H. Friend, P.L. Burns, and A.B. Holmes,*Light-emitting diodes based on conjugated polymers*. Nature, 347, 539-541 (1990).

[3] G.W. Gray, S.M. Kelly, *Liquid crystals for twisted nematic display devices*. J. Mater. Chem., 9, 2037-2050 (1999).

[4] http:en.wikipedia.org/wiki/Adhesive. Retrieved on 08062007.

[5] R.J. Young and S.J. Eichhorn, *Deformation mechanisms in polymer fibres and nanocomposites*. Polymer, 48, 2-18 (2007).

[6] Q. Yuan and R.D.K. Misra, *Polymer nanocomposites: current understanding and issues*. Mats. Sci. Tech., 22(7), (2006).

[7] J. Njuguna and K. Pielichowski, *Polymer Nanocomposites for Aerospace Applications: Properties*. Adv. Engin. Mats., 5(11), (2003).

[8] M. Meador, *Recent Advances in the Development of Processable High-Temperature Polymers*. Annu. Rev. Mater. Sci., 28, 599-630 (1998).

[9] S.A. Safran, *Statistical Thermodynamics of Surfaces, Interfaces, and Membranes*. Addison-Wesley, Reading, MA. (1994).

[10] A.Y. Grosberg and A.R. Khokhlov, *Statistical Physics of Macromolecules*. AIP, New York, (1994).

[11] D.P. Landau and K. Binder, *A Guide to Monte Carlo Simulations in Statistical Physics* Cambridge University Press, Cambridge, (2000).

[12] A.J. Kinloch, et. al, *The effect of silica nano particles and rubber particles on the toughness of multiphase thermosetting epoxy polymers*. J. Mat. Sci. Lett., 0022-2461, (2005).

[13] M. Rubenstein and R.H. Colby, *Polymer physics*. New York: Oxford University Press (2003).

[14] M. Doi and S.F. Edwards, *The theory of polymer dynamics*. New York: Oxford University Press (1986).

[15] K. Kremer and G. Grest, *Entanglement in polymer melts and networks*. In: K. Binder, editor. Monte Carlo and molecular dynamics simulations in polymer science. New York: Oxford University Press, p. 194-271 (1995).

[16] J. Baschnagel, K. Binder, P. Doruker, A. Gusev, O. Hahn, K. Kremer, et al., *Bridging the gap between atomistic and coarse-grained models of polymers: status and perspectives*. Adv. Polym. Sci. 152, 41-156, (2000).

[17] W. Paul and G. Smith, *Structure and dynamics of amorphous polymers: computer simulations compared to experiment and theory*, Rep. Prog. Phys., 67, 1117-85, (2004).

[18] P.G. de Gennes, *Scaling concepts in polymer physics*. Ithaca, New York: Cornell University Press (1979).

[19] D.N. Theodorou, U.W. Suter, *Detailed Molecular Structure of a Vinyl Polymer Glass*. Macromolecules, 18(7), (1985).

[20] K. Kremer, G.S. Grest, and I. Carmesin, *Crossover from Rouse to Reptation Dynamics: A Molecular-Dynamics Simulation*. Phys. Rev. Lett., 61(5), (1988).

[21] E. Leontidis, B. Forrest, A. Widmann, and U. Suter, *Monte Carlo Algorithms for the Atomistic Simulation of Condensed Polymer Phases*. J. Chem. Soc. Faraday Trans., 91(16), 2355-2368 (1995).

[22] K. Kremer and G.S. Grest, *Dynamics of entangled linear polymer melts: A molecular-dynamics simulation.* J. Chem. Phys., 92, 5057 (1990).

[23] M. Muller and L.G. MacDowell, *Interface and surface properties of short polymers in solution: Monte Carlo simulations and self-consistent field theory.* Macromolecules, 33(10), 3902-3923 (2000).

[24] K. Kremer, *Computer Simulations for Macromolecular Science*. Macromol. Chem. Phys., 204, 257-264 (2003).

[25] F. Muller-Plathe, *Coarse-graining in polymer simulation: From the atomistic to the mesoscopic scale and back*. Chem. Phys. Chem., 3, 754-769, (2002).

[26] J.T. Padding and W.J. Briels, *Time and length scales of polymer melts studied by coarse-grained molecular dynamics simulations*. J. Chem. Phys., 112(2), (2002)

[27] K. Binder and W. Paul, *Monte Carlo Simulations of Polymer Dynamics: Recent Advances*. J. Polymer Science B, 35, 1-31 (1997).

[28] S. Glotzer and W. Paul *Molecular and Mesoscale Simulation Methods for Polymer Materials*. Annu. Rev. Mater. Res., 32, 401-436, (2002).

[29] E.F. Oleinik, *Plasticity of Semicrystalline Flexible-Chain Polymers at the Microscopic and Mesoscopic Levels*. Polymer Sci. C, 45(1), 17-117, (2003).

[30] D.K. Muravin, V.G. Oshmyan, *Simulation of particulate-filled composite deformation diagrams on the basis of a constitutive model of large plastic deformation for a polymer matrix*. J. Macromol. Sci. Phys., B38(5-6), 749, (1999).

[31] K.P. Hermann, V.G. Oshmyan, S.A. Timman, and M.Y. Shamaev, . Polymer. Sci. C., 44(1), 63, (2002)

[32] V.G. Oshmyan, S.A. Timman, and M.Y. Shamaev, *Modeling of ductile failure of polymer blends and composites with account of interface formation*. Polymer. Sci. A. 45(10), 1011-1019, (2003)

[33] F. Guild, Private Communications (2007).

[34] A. Hausrath and A. Goriely, *Repeat protein architectures predicted by a continuum representation of fold space*. Protein Sc., 15(4), 753-760, (2006).

[35] R. Harris and J. Hearst, *On polymer dynamics*, J. Chem. Phys., 44(7), (1966).

[36] R. Goldstein and S. Langer, *Nonlinear dynamics of stiff polymers*. Phys. Rev. Lett., 75(6), (1995).

[37] R. Goldstein, T. Powers, and C. Wiggins, *Viscous Nonlinear Dynamics of Twist and Writhe*. Phys. Rev. Lett., 80(23), (1998).

[38] O. Kratky and G. Porod, *Röntgenuntersuchung gelöster Fadenmoleküle (translated as: X-ray examination of solved filamentary molecules)*. Rec. Trav. Chim., 68, (1949).

[39] S.F. Edwards and K. Freed, *Theory of Dynamical Viscosity of Polymer Solutions*. J. Chem. Phys., 61, 1189, (1974).

[40] A. Bru, et. al. *Super-Rough Dynamics on Tumor Growth*. Phys. Rev. Lett., 81(18), (1998).

[41] A. Bru, et. al. *Pinning of Tumoral Growth by Enhancement of the Immune Response*. Phys. Rev. Lett., 92(23), (2004)

[42] A. Chua, *Notes on the Motion of Curves*. (Unpublished).

[43] H. Hasimoto, *A soliton on a vortex filament*. J. Fluid Mech., 51(3), (1972).

[44] K. Han, *Curve motions from the integrable equations having variable spectral parameters*. J. Phys. A: Math. Theory, 40, (2007).

[45] C. Canuto, M.Y. Hussaini, A. Quarteroni, and T.A. Zang, *Spectral Methods in Fluid Dynamics*. Springer-Verlag, New York, 1988.

[46] H.C. Andersen, *Rattle: A "Velocity" Version of the Shake Algorithm for Molecular Dynamics Calculations*. J. Comp. Phys., 52, 24-34 (1983).

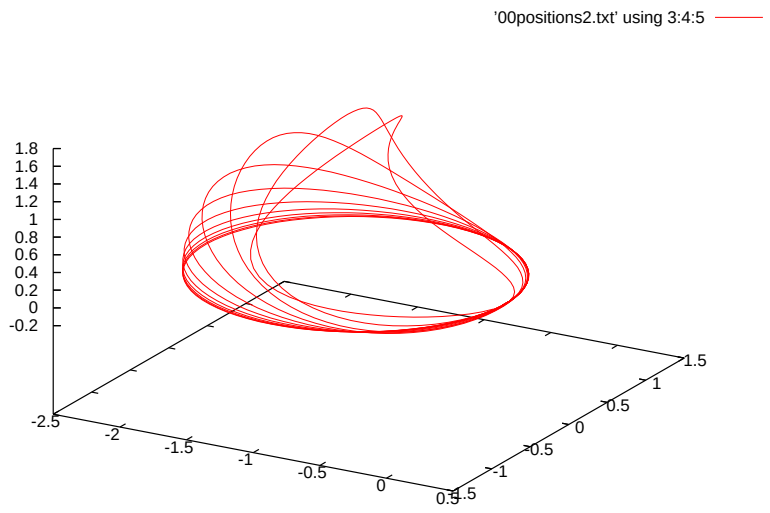

Figure 1: Hasimoto dissipative dynamics: Shape relaxation

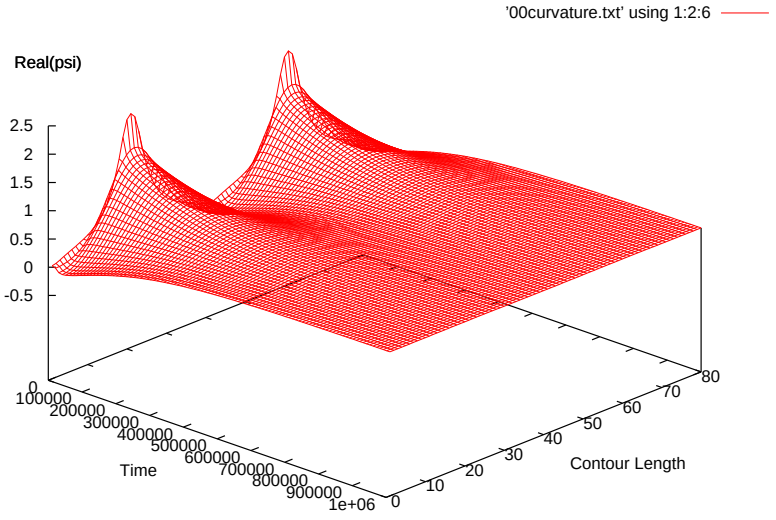

Figure 2: Hasimoto dissipative dynamics: Relaxation of the real component of ψ

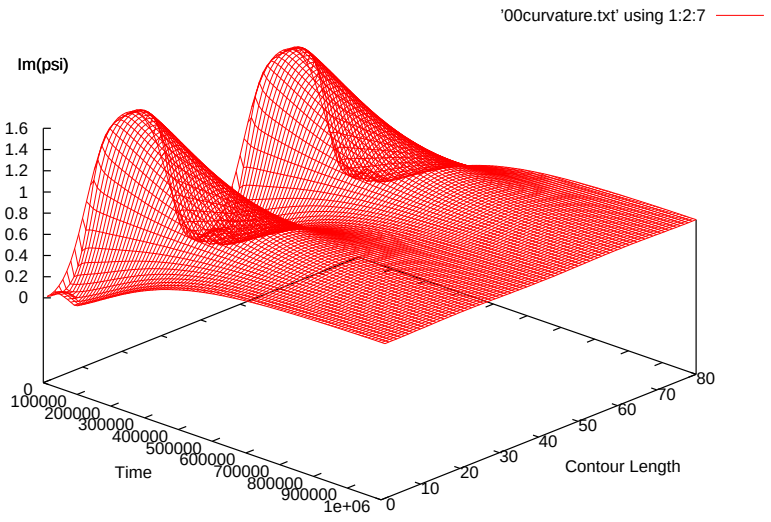

Figure 3: Hasimoto dissipative dynamics: Relaxation of the imaginary component of ψ

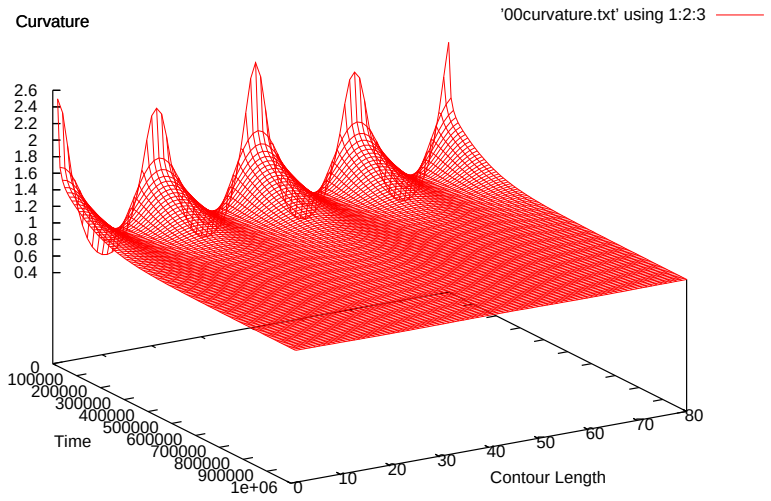

Figure 4: Hasimoto dissipative dynamics: Relaxation of the real curvature, $\tilde{\kappa}$

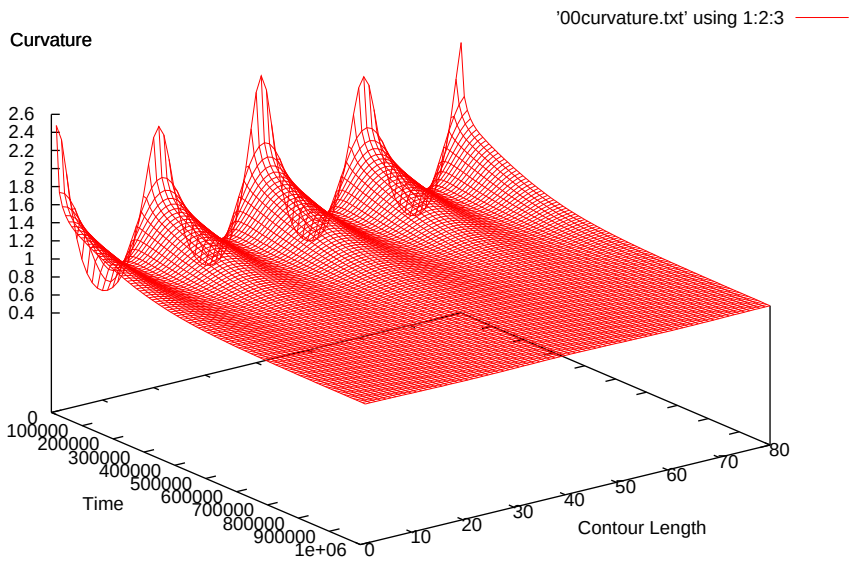

Figure 5: Discrete dissipative dynamics: Curvature relaxation